JACS
JOURNAL OF THE AMERICAN CHEMICAL SOCIETY

pubs.acs.org/JACS

Article

Protective Layers Based on Carbon Paint To Yield High-Quality Large-Area Molecular Junctions with Low Contact Resistance

Senthil Kumar Karuppannan, Esther Hui Lin Neoh, Ayelet Vilan,* and Christian A. Nijhuis*

Cite This: J. Am. Chem. Soc. 2020, 142, 3513−3524

Read Online

ACCESS | Metrics & More | Article Recommendations | Supporting Information

ABSTRACT: A major obstacle for transforming large-area molecular junctions into a viable technology is the deposition of a top, metallic contact over the self-assembled monolayer (SAM) without chemically damaging the molecules and preventing an interface-limited charge transport. Often a thin conducting layer is softly deposited over the SAM to protect it during the deposition of the metal electrode which requires conditions under which organic molecules are not stable. We report a new protective layer based on carbon paint which is highly conductive and has metallic-like behavior. Junctions made of SAMs of *n*-alkanethiolates supported by Au were characterized with both dc and ac techniques, revealing that carbon paint protective layers provide a solution to three well-known challenges in molecular junctions: series resistance of the leads, poor interface conductance, and low effective contact area related to the roughness of the interfaces. Transport is constant with coherent tunneling down to 10 K, indicating the carbon paint does not add spurious thermally activated components. The junctions have both high reproducibility and good stability against bias stressing. Finally, normalized differential conductance analysis of the tunneling characteristics of the junctions as a function of molecular length reveals that the scaling voltage changes with molecular length, indicating a significant voltage drop on the molecules rather than on the molecule−electrode interface. There is a clear inverse dependence of the scaling voltage on length, which we deduced has a tunneling barrier height of close to 2 eV. The paper establishes the reliability of carbon paint protective layers and provides a procedure for discriminating genuine molecular effects from interfacial contributions.

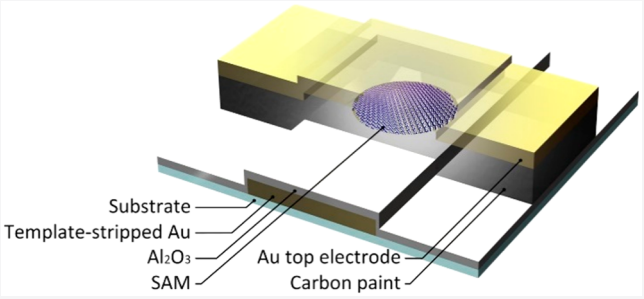

INTRODUCTION

Molecular tunnel junctions work at the nanoscale where quantum effects dominate and are in many ways complementary to existing technologies.[1−5] Large-area junctions are based on self-assembled monolayers (SAMs), or monolayers of covalently linked molecules, and are, unlike single-molecule junctions, in principle scalable.[5] It remains challenging, however, to fabricate these junctions on large scales as the SAMs are not stable under typical fabrication conditions. To avoid damage to the SAMs during fabrication and to block diffusion of metallic atoms and associated formation of metal filaments, conductive protective layers (PLs) on the monolayers have been used, such as conductive polymers,[3,6,7] electron-beam-deposited carbon (e-C),[8,9] nanoparticles coated with a thick layer of polymer,[10] multilayer graphene (MLG),[11−13] or reduced graphene oxides (rGO),[14] but they introduce artifacts such as series resistance that limits the minimum SAMs thickness that can be measured and unwanted temperature effects in the electrical characteristics of the junctions; in addition, some PLs limit scalability (see Table 1). This paper describes a new PL based on carbon paint (CP) with the following advantages: (i) it can be directly spin coated onto SAMs and protects the SAM during thermal deposition of the Au top contacts, (ii) it does not introduce temperature effects in the tunneling characteristics of the junctions down to 8.5 K, (iii) it can be readily incorporated in existing, scalable fabrication processes, (iv) it has a very low contact resistance (R_0) with the SAMs, (v) it does not introduce stray capacitances (C_{stray}), and (vi) it does not suffer from parasitic currents across the CP layer. Using normalized differential conductance (NDC) analysis,[15−17] we show that the voltage primarily drops over the molecules, ensuring that molecular effects dominate the electrical characteristics. These features make the CP a potentially important PL for applications in molecular electronics.

It is well known that metal contacts cannot be directly deposited onto the SAMs due to damage induced by the impinging metal atoms and clusters and the typically high processing temperatures encountered in metal deposition,[2,18] apart from a few notable exceptions.[18−21] For this reason, a large number of alternative fabrication techniques have been proposed, but most of them suffer from one or more

Received: November 18, 2019
Published: January 17, 2020

https://dx.doi.org/10.1021/jacs.9b12424
J. Am. Chem. Soc. 2020, 142, 3513−3524

Table 1. Characteristics of the Different Types of Large-Area Junctions with $S(CH_2)_{n-1}CH_3$ or $S(CH_2)_nS$

type of junction/technique	PL[a]	PL-induced T effect	scalable	β (n^{-1})	$\log_{10}(J_0)$ at 0.5 V [A/cm^2]	fractional coverage[n] $\log_{10}\frac{A_{elec}}{A_0}$	ref
large area/micropore	MLG[b]	no	no	1.06 ± 0.14	~8.3[c]	−0.6	11,27
large area/micropore	rGO[d]	yes	yes	1.27−0.82	4.0−6.3	−5 to −2.5	12,14,71
large area/micropore	mGO[e]	no	yes	0.89 ± 0.05	~7.0[c]	−2	31,33,72
large area/micropore	PEDOT:PSS[f]	yes	yes	0.45−0.77	5.0−8.6	−4 to −0.3	6,68,69
large area/EGaIn	GaO_x[g]	no	limited	0.80−0.94	2−4.2	−7 to −4.5	25,73
large area/micropore	NP-PVP[h]	no	yes	1.00 ± 0.20	~5.0[c]	−4	10
large area/direct metal deposition	NA[i]	NA	yes	1.05 ± 0.08	~8.7[c]	−0.2	47,74
large area/micropore	CP[j]	no	yes	1.08 ± 0.05	6.2 ± 0.5	−2.7 ± 0.5	this work
large area/micropore	e-C[k]	yes	yes	NA	NA	NA	8,59,75
small area/(STM[l])	NA	NA	no	1.02 ± 0.14	~8.9[c]	0	50,51
small area/(AFM[m])	NA	NA	no	1.10 ± 0.1	~8.2[c]	−0.7	58,63
single-molecule junction/STM	NA	NA	no	0.51−1.09	NA	NA	50,51,76,77

[a]PL is a protective layer. [b]MLG is multilayer graphene. [c]Roughly estimated from the $J(V)$ curves in the corresponding references. [d]rGO is reduced graphene oxide. [e]mGO is monolayer graphene oxide. [f]PEDOT:PSS is poly(3,4-ethylene dioxythiophene) polystyrenesulfonate. [g]GaO_x is gallium oxide. [h]NP-PVP is nanoparticles (NP) stabilized with a polyvinylpyrrolidone (PVP). [i]NA means "not applicable". [j]CP is carbon paint. [k]e-C is electron-beam-deposited carbon film. [l]STM is scanning tunneling microscopy. [m]AFM is atomic force microscopy. [n]Fractional coverage is estimated according to $A_{elec}/A_0 = J_0 a_{mol}/(G_0 V \tau_C)$, with a_{mol} = 22 Å^2, G_0 = 0.77 μS, V = 0.5 V, and τ_C = 0.05.

disadvantages (see Table 1 for a brief overview). To avoid direct metal deposition onto the SAMs, liquid−metal electrodes, such as Hg[22,23] and eutectic gallium−indium alloy (EGaIn),[24,25] have been used, but such junctions lack the mechanical stability required for potential applications. Akkerman et al.[26] used a conductive polymer poly(3,4-ethylene dioxythiophene) polystyrenesulfonate (PEDOT:PSS) as a PL, but this approach only works for hydrophilic SAMs, and the PEDOT:PSS film itself adds a thermally active component to the junction characteristics. Puebla-Hellmann et al.[10] proposed Au nanoparticles stabilized with a 3 nm thick layer of polyvinylpyrrolidone as a PL, but the role of the polyvinylpyrrolidone and how it interacts with SAMs are unknown. Lee et al.[11,27] showed that MLG is an interesting PL, but large-scale transfer of MLG obtained by chemical vapor deposition on Cu is still a technological challenge, and the presence of residual polymers (used for transfer) and Cu complicates reproducibility.[28,29] Others have used solution-exfoliated graphene and rGO,[30−33] but the role of the ions within the graphene layers is not understood.

Carbon paints, also called carbon inks, are cost effective, readily available, and highly conductive.[34,35] They are based on suspensions of 0.2−2 μm graphite particles (carbon black is a mixture of carbon-based materials obtained from incomplete combustion) in organic solvents (such as isopropanol, water, or methyl ethyl ketone).[9,36−38] These CPs may contain, besides an organic solvent, a stabilizing polymer (such as cellulose resin, fluoroelastomer, poly(acrylic acid), polyvinyl butyral, or polyimide siloxane)[36−38] and therefore require curing at elevated temperatures (65−150 °C) to yield conductive films (of 0.02−1.20 kΩ/sq depending on the thickness of the films typically ranging from 2 to 25 μm).[36,37] The surface roughness and resistivity of the CP films typically vary from 2.5 nm to 5.0 μm[35,38−43] and from 5.7 × 10^{-4} to 11.7 × 10^{-4} Ω cm, respectively.[44] CPs without stabilizing polymers[37] are available and form highly conductive films simply by drying in air (thus annealing is not required). These materials can be readily spin coated, inkjet printed, or spray coated on various substrates (e.g., plastics, paper, or metal) and have been used to fabricate flexible, wearable, diagnostic, and foldable electronic devices.[45,46] Therefore, the CPs are interesting to explore as protective barriers for applications in molecular electronics.

The conductance, G, of a molecular junction is generally described in terms of transmission probability, τ, which can be further divided into the probability to cross the two interfaces τ_C and the molecular body τ_{mol}[47]

$$G = NG_0 \cdot \tau_C \tau_{mol} \quad (1)$$

The overall conductance is a summation of the transmission through N noninteracting molecules with a maximal conductance of the quantum of conductance, G_0 (= 0.77 μS). In practice, the measured quantity is often the current density J (in A/cm^2) rather than G ($J = GV/A_0$, where V = voltage; A_0 = geometrical area), and different junction configurations are commonly compared using eq 2

$$\log_{10}|J| = \log_{10}|J_0| - \beta d/2.303 \quad (2)$$

where β is the tunneling decay coefficient (per carbon number, n^{-1}), d is the width of the tunneling barrier (i.e., the length of the molecules in n), and J_0 (A/cm^2) is a pre-exponential factor. The consensus value of β for alkanethiolate ($S(CH_2)_{n-1}CH_3$, or SC_n in short) based junctions falls in the range of 0.95−1.10 n^{-1}, but high or low values of β are associated with defective junctions (Table 1).[48,49] Table 1 also shows that the values of J_0 vary orders magnitude from 10^2 to 10^9 A/cm^2 across the different junction platforms, but it seems that ~10^9 A/cm^2 is the upper limit which has been observed for single-molecule junctions[50,51] and junctions with graphene electrodes.[11,27] Comparing eqs 1 and 2 and taking $\tau_{mol} \propto e^{-\beta d/2.3}$ yields the following expression for J_0

$$J_0 = \frac{A_f}{a_{mol}} G_0 V \cdot \tau_C \cdot f(R_s) \quad (3)$$

which identifies three main sources in the variations in J_0: (i) the unknown fraction of the junction area, A_f, across which the current flows, (ii) the unknown value of τ_C,[52,53] and (iii) the series resistance of the PL, R_s. The fraction of the junction area, A_f, is defined as the ratio between the effective electrical

https://dx.doi.org/10.1021/jacs.9b12424
J. Am. Chem. Soc. 2020, 142, 3513−3524

contact area, $A_{elec} = N \cdot a_{mol}$ (where a_{mol} is the molecular footprint), and the nominal, geometrical area of the junction, A_0[54,55]

$$A_f = A_{elec}/A_0 \quad (4)$$

Consequently, values of A_f can be $10^{-3}-10^{-6}$ due to the surface roughness of the electrodes;[56,57] the interface transmission (τ_C) of covalent molecule−electrode contacts is about 2 orders of magnitude higher than that of physisorbed contacts.[52,58] The functional effect of the series resistance, $f(R_s)$, follows standard electronics ($G_{tot} = \frac{G_{mol}}{1 + R_s G_{mol}}$) and is negligible for $R_s \ll 1/G_{mol}$. There is a fundamental difference between the contact transmission, τ_C, and R_s. Unlike R_s, τ_C is part of the coherent tunneling process and does not behave as an independent resistor; therefore, τ_C cannot be accounted for by standard methods such as four-probe measurements, as is common practice with R_s. Therefore, it is nontrivial to account for the change in τ_C induced by the PL or to separate τ_C from changes in A_f.

In principle, the PL can affect both τ_C and R_s: ineffective coupling or limited density of states reduce τ_C, while the charge carrier mobility through the CP affects R_s. The value of R_s limits the minimum SAM thickness (or value of n in the case of junctions with SC_n SAMs) that can be measured. For instance, junctions with PDOT:PSS,[26] e-C,[59] and rGO[12,14] are limited to $n \geq 8$. Here, we show that CP-PL yields junctions with SAMs of SC_n with $\beta = 1.09 \pm 0.04$ n^{-1} and a high J_0 of $10^{6.20\pm0.53}$ A/cm^2. We observe a high τ_C and low R_s resulting in a low enough overall CP-induced resistance to enable one to measure thin SAMs with $n \geq 4$. A high effective contact area with the SAM due to efficient wetting of the SAM by the CP explains the observed improvement in τ_C. To the best of our knowledge, this paper describes for the first time three different roles of the contact and evaluates them quantitatively. Acknowledging and learning how to control them are important toward the continuous effort of the community to improve molecular junctions.

RESULTS AND DISCUSSION

Fabrication of the Devices. Figure 1 shows a schematic illustration of the junctions (we fabricated 132 junctions per 1.0×1.0 cm^2) where the CP layer protects the SAM inside the micropores during deposition of the Au top electrode. The micropores (with a diameter of 10 μm) were fabricated in AlO_x on an ultrasmooth template-stripped Au (Au^{TS}) bottom electrode obtained with template stripping using a previously reported procedure.[60] Since in template stripping a glue (Norland No. 61) is used, the fabrication process has to be performed at low temperature and using solvents that are compatible with the glue.

Figure 2 shows all of the fabrication steps of the devices. Briefly, Au (150 nm) was deposited on a Si wafer with its native SiO_2 layer by shadow mask deposition (Figure 2A) followed by template striping (Figure 2B and 2C). On the entire surface, 35 nm Al_2O_3 was deposited by atomic layer deposition at 90 °C (Figure 2D) followed by spin coating of poly(methyl methacrylate) (PMMA) and patterning with electron-beam lithography. Then we etched 10 ± 0.5 nm of Al_2O_3 by deep reactive ion etching to form micropores (Figure 2E) followed by removal of the PMMA by cleaning with O_2 plasma (3 min, pressure ≈ 10^{-2} mbar). In the second etching step with aqueous NH_4F (40%), the Al_2O_3 was etched through

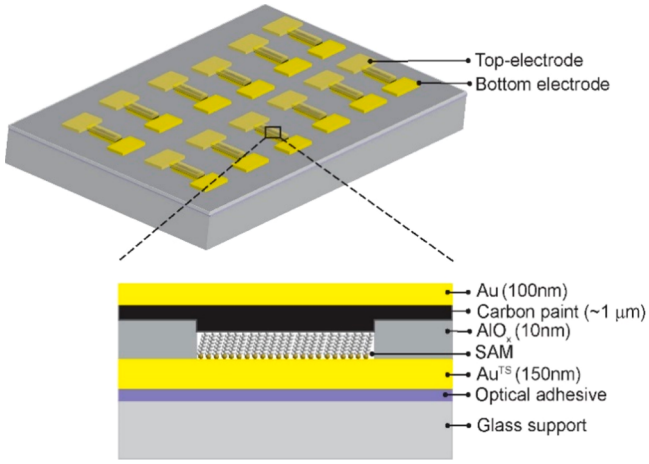

Figure 1. Schematic illustration of the molecular tunnel junction ($Au^{TS}-SC_n//CP//Au$) with carbon paint (CP) as a protective layer: TS indicates template stripped, "−" indicates a covalent interface, and "//" indicates a noncovalent interface.

to expose the Au^{TS} surface (Figure 2F). The SAMs were formed by immersion of the substrates in the corresponding ethanolic solutions of the mercaptoalkanethiols (Figure 2G). The CP was spin coated on the entire sample at 6000 rpm (Figure 2H) followed by deposition of the Au top electrode by shadow mask deposition (Figure 2I) after which the excess CP was removed by oxygen plasma etching (Figure 2J).

Characterization of Protection Layer. The CP we used was obtained from Structure Probe Inc. (SPI) and is based on graphite flakes suspended (density = 0.88 kg/L) in isopropanol, which forms films with a sheet resistance of 1.2 kΩ/sq for 25 μm thick films[37] (for our application, however, the vertical resistance is important to consider as discussed below). We chose this CP for the following 5 reasons: (i) it does not require annealing as the isopropanol readily evaporates during spin coating (SAMs decompose at elevated temperatures of >340 K),[61,62] (ii) it does not contain stabilizing polymers which may intercalate with the SAM and introduce additional resistances and unwanted temperature effects in the junction, (iii) it is well defined and only consists of graphite flakes unlike inks based on carbon black (which is essentially soot) or (reduced) graphene oxides which are highly defective and contain ions used for exfoliation, (iv) it is highly solution processable, the suspension is highly stable (see Figure S1), and its viscosity can be easily tuned by simply diluting with isopropanol, and (v) it has a work function of 4.34 ± 0.05 eV (Figure 3A) which is close to that of the Au electrode coated with a SAM (4.2 eV).[63] To reduce the film thickness, we diluted the CP by a factor of 5 with freshly distilled isopropanol (which leaves no solid residues upon evaporation) followed by spin coating at 6000 rpm to yield a film thickness of 1.0 ± 0.2 μm measured using a profilometer (see Section S1, Figure S2). Figure 3B shows the scanning electron microscopy (SEM) image of the CP layer. The SEM image shows that the CP forms a continuous film of graphite flakes (inset of Figure 3B), and we determined the size distribution of the graphite flakes from SEM images recorded on dilute layers of CP on Au^{TS} (see Section S1 and Figure S3). The size of graphite flakes is 0.18−0.20 μm, which is independent of the lot number of this commercially available CP. To investigate the surface roughness of the $Au^{TS}-SAM//CP$ interface, we deposited CP on Au^{TS} supporting a SAM of

https://dx.doi.org/10.1021/jacs.9b12424
J. Am. Chem. Soc. 2020, 142, 3513−3524

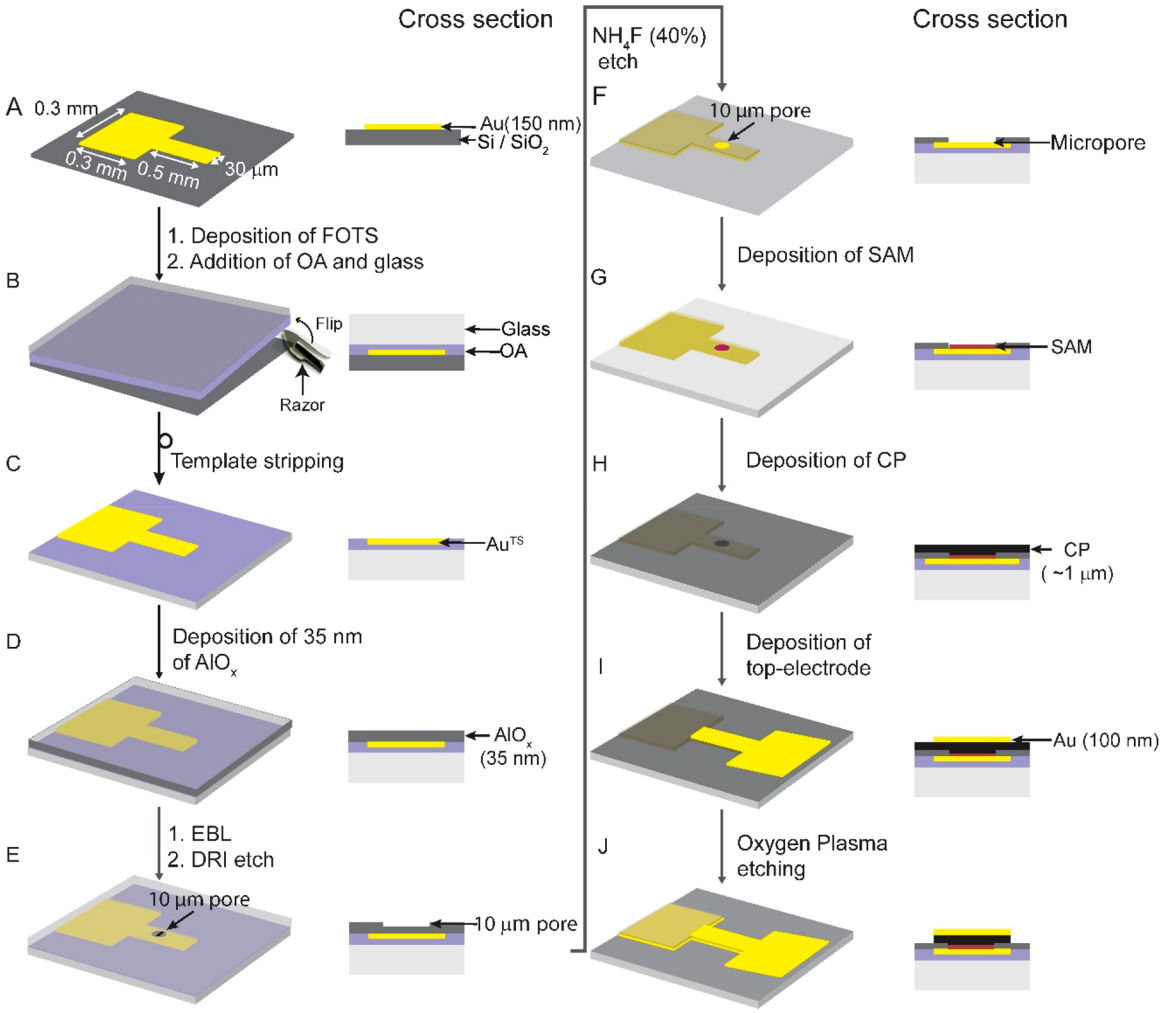

Figure 2. Fabrication process of the Au^{TS}–SC_n//CP//Au junctions based on SAMs on template-stripped Au inside micropores (with a diameter of 10 μm) with a carbon paste (CP) protective layer and Au top contacts. All fabrication steps are explained in the main text.

SC_{12} and then used Scotch tape to remove the CP film from the Au^{TS} surface and expose the CP film that had been in contact with the Au surface (see Section S1); this template-stripped CP film was imaged by tapping mode atomic force microscopy (AFM). The AFM image (Figure 3C) reveals a root-mean-square surface roughness of 2.1 ± 1.0 nm measured over an area of 1.0 × 1.0 μm^2 (Figure S5 shows the line profiles) which falls in the range of previously reported values for exfoliated graphene and rGO films.[35,39−43] The line profiles reveal the presence of "pits" with a depth of 20 nm, which are about 50 times smaller than the thickness of the CP film; this indicates that the CP layer forms a continuous film and that the Au top electrode cannot form direct contacts with the SAM. The area available to form electrical contact is estimated from AFM image analysis of each surface using nasoscope software as reported before.[55] The AFM image of the CP layer (Figure S6C) yields an available area of 13%. For the bottom electrode, Figure S3 shows the AFM image of Au^{TS}–SAM inside micropores (with a diameter of 10 μm) and the estimated area available to form electrical contact is ∼11% of the geometrical surface area of the bottom electrode (Figure S6B). Thus, the value of A_f for the junction (i.e., multiplication of available area for the top and bottom electrode) is on the order of $\sim 10^{-2}$, which is about a 2 orders of magnitude improvement over cone-shaped tip EGaIn junctions for which $A_f = 10^{-4}$. This observation can be explained as the graphite flakes are likely deposited in a parallel orientation with respect to the SAM during spin coating.

X-ray photoelectron spectroscopy (XPS) was used to study the chemical composition of the template-stripped CP film. We carried out the XPS measurements on freshly template-stripped CP films from Au^{TS} supporting a SAM of SC_{12} which were cleaned in situ by mild sputtering with argon ions at low acceleration voltages (1.0 kV, 0.1 μA, 300 s). To determine the batch-to-batch consistency of the CP^{TS} films, we measured XPS from CP^{TS} films prepared from the three different batches of CP (lot numbers 1220501, 1230420, and 1239429). Figure S7 shows the XPS survey scans of template-stripped CP films before and after cleaning with Ar sputtering, Figures S8 and S9 show the corresponding high-resolution C 1*s* and O 1*s* XPS spectra; see section S2 for detailed analysis. The survey scans (Figure S7) show a strong C 1s peak at 284.3 eV, a O 1s peak at 532.4 eV, and a weak O(KLL) Auger band between 955 and 985 eV, but Au 4f and S 2p signals are absent (from which we conclude that Au and the SAM remained intact during template stripping of the CP layer). The amount of oxygen decreased from 15 ± 2% to 5 ± 1% after in situ sputter cleaning. This decrease in oxygen content indicates the presence of adventitious materials on the ex-situ-prepared CP films. The residual 5% oxygen in the CP film may originate

https://dx.doi.org/10.1021/jacs.9b12424
J. Am. Chem. Soc. 2020, 142, 3513−3524

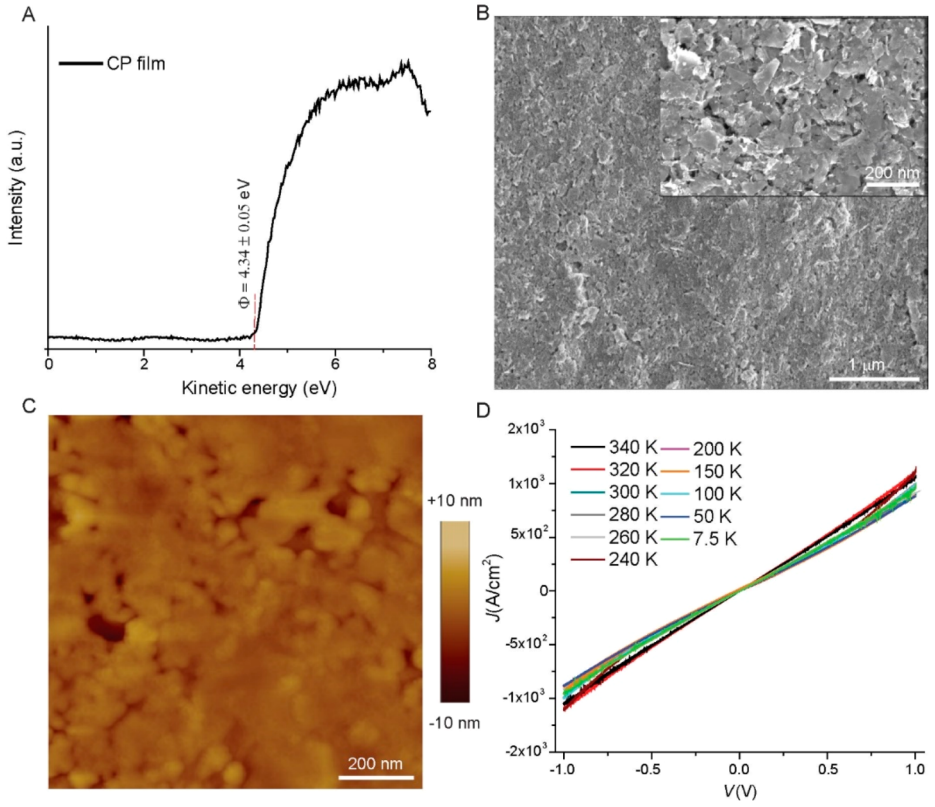

Figure 3. (A) Ultraviolet photoelectron spectra of the CP film which was obtained by templating the CP film from Au^{TS}–SC_{12} with Scotch tape. (B) Scanning electron microscopy image of spin-coated CP film. (C) Atomic force microscope image of CP, which was obtained by template stripping the CP film from Au^{TS}–SC_{12} with Scotch tape. (D) $J(V)$ characteristics of a Au^{TS}//CP//Au junction as a function of temperature.

from the solvent (isopropanol), which contains an OH group (although its presence under ultrahigh-vacuum conditions is unlikely), or physisorbed water or oxygen introduced during preparation of the CP films (e.g., during spin coating in ambient conditions),[64] or small amounts of carbon oxide.

For our application, it is important to determine the temperature-dependent behavior and to quantitfy the vertical resistance of the CP film since it is placed in series with the SAM. Figure 3D shows the $J(V)$ characteristics of an Au^{TS}//CP//Au junction without a SAM with a ~1.0 μm thick layer of CP as a function of temperature (see Section S3, Figure S10). Changes in the applied temperature did not have a significant effect on the $J(V)$ characteristics. The vertical resistance of the CP layer is 0.012 Ω (resistivity = 0.10 Ω cm), which was determined with four-wire (Kelvin) measurements (see Figure S10B). This resistivity is similar to e-C (0.17 Ω cm), which is deposited onto covalently grafted monolayers by sputtering in a vacuum,[59] but CP has the advantage of solution processability similar to that of rGO.[14] The CP has a factor of 3–5 higher resistivity than GO (0.018 Ω cm)[65] or PEDOT:PSS[26] (0.033 Ω cm), which is likely caused by the relatively thick CP film we used here of 1 μm, yet these alternative PLs suffer from residual ions (dangling OH and ionized PSS, respectively), and their resistivity depends on the temperature (see Table 1).[14,60,65,66]

ELECTRICAL CHARACTERIZATION OF THE JUNCTIONS

To determine the value of β of the Au^{TS}–SC_n//CP//Au junctions, we measured 10–20 $J(V)$ curves across 66–150 junctions for each value of n = 4, 6, 8, 10, 12, and 14 (Table S1). Using previously reported methods,[67] we determined the Gaussian log-average current densities, $\langle \log_{10}|J| \rangle_G$, for each measured applied voltage (V) (see Section S4, Figure S11) which were used to construct the $\langle \log_{10}|J| \rangle_G$ vs V curves. Figure 4A shows the semilog plots for all values of n. The values of the Gaussian log-standard deviations, $\sigma_{\log,G}$, are small (average of 0.32), which indicates that the reproducibility of the junctions is very good. The yield of nonshorting junctions is 100%, from which we conclude that the CP layer effectively protected the SAM during fabrication of the top electrode. The average yield in working junctions is 74.8% (nonworking junctions were open circuits due to fabrication errors), which is similar to other techniques.[5,6,10,25,26,48,68]

Figure 4B shows that the $\langle \log_{10}|J| \rangle_G$ values decrease linearly as n increases from 4 to 14, but the values of $\langle \log_{10}|J| \rangle_G$ for junctions with n = 4 are similar to those for a control junction lacking the SAM, i.e., Au^{TS}//CP//Au junction (but junctions with thinner SAMs are limited by the resistance of the CP layer); below we show that junctions with n = 4 are dominated by molecular effects. The resistance of conductive polymers and graphene oxide protective barriers limited the thinnest SAM that could be measured to $n \geq 8$;[12,14,26,59] hence, CP protective barriers offer a significant benefit allowing for measurements of thin SAMs with $n \geq 4$.

Fitting the data at +0.5 V in Figure 4B to eq 2 yields β = 1.09 ± 0.04 n^{-1} and $\log_{10}|J_0|$ = 6.20 ± 0.53 A/cm^2, and a fit to the +0.05 V data of Figure 4B yields β = 1.10 ± 0.05 n^{-1} and $\log_{10}|J_0|$ = 5.17 ± 0.36 A/cm^2 (errors represent the 95% confidence levels).[11,27] The value of β is very close to previously reported values of β for junctions with n-alkanethiolate SAMs, but the value of $\log_{10}|J_0|$ is high. The

https://dx.doi.org/10.1021/jacs.9b12424
J. Am. Chem. Soc. 2020, 142, 3513–3524

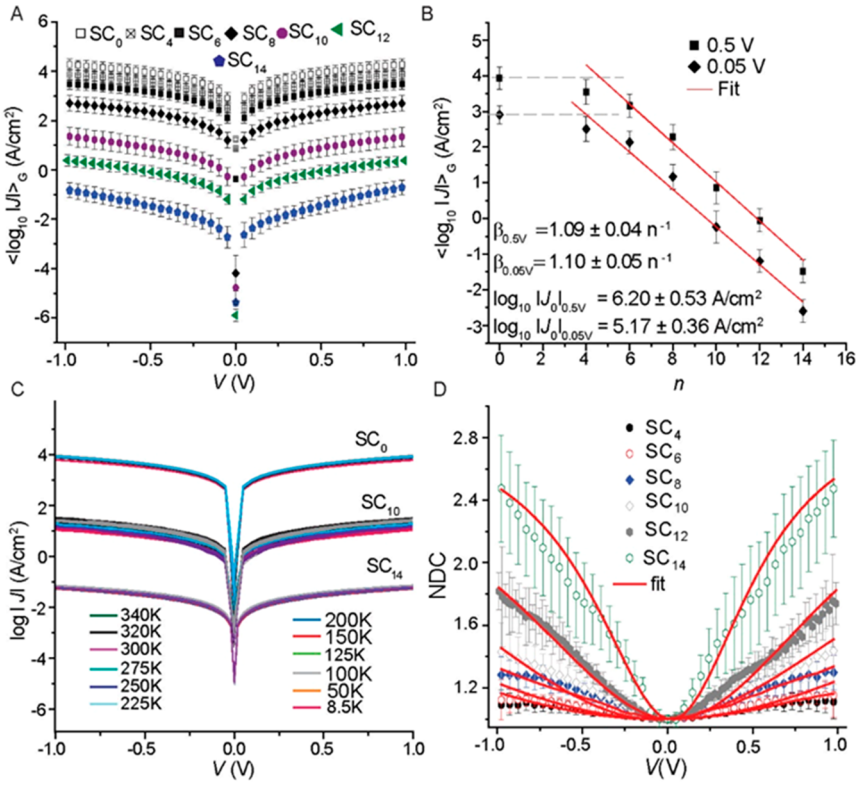

Figure 4. (A) $\langle \log_{10}|J| \rangle_G$ vs V traces of Au^{TS}–SC_n//CP//Au junctions. (B) Value of $\langle \log_{10}|J| \rangle_G$ (measured at V = +0.5 and +0.05 V) plotted against the number of carbons, n; dashed gray lines indicate the current across the control device without a SAM; red solid lines are fits to eq 2. (C) $J(V)$ characteristics as a function of T for junctions with n = 10 or 14 or without a SAM for T = 8.5–340 K. (D) Normalized differential conductance vs V for junctions with n = 4, 6, 8, 10, 12, and 14. Error bars represent 99% confidence levels, and solid red lines are fit to eq 5.

values of $\log_{10}|J_0|$ differ by ~1 (in $\log_{10}$ units), reflecting a factor of 10 in the applied voltage (see eq 3). Table 1 shows that the values of $\log_{10}|J_0|$ vary across the different junction platforms, but it seems that ~10^9 A/cm^2 is the upper limit which has been observed for single-molecule junctions[50,51] and junctions with graphene electrodes,[11,27] while a slightly lower value is observed for junctions with MLG layers and junctions without PL prepared by direct metal deposition, STM, and cp-AFM-based junctions. The second-last column of Table 1 provides an estimate for the value of A_f based on eq 3 with standard values; the value of τ_C = 0.05 was chosen to yield a perfect coverage (i.e., A_f = 1) for the highest reported J_0 for junctions with a STM tip as the top electrode. It suggests a fractional coverage of 0.002 (which is very close to the value estimated from the AFM images (Figure S6) discussed earlier) for CP-protected molecular junctions, which is at the high end of large-area junctions, except for MLG.

Table 1 also shows that the variation of β is large, and some techniques yield β values as low as 0.45 n^{-1} or as high as 1.27 n^{-1}, which clearly indicates that those junctions suffered from defects.[49,70] Thus, the CP protects the SAMs during the fabrication process efficiently without introducing defects that compromise the value of β while maintaining medium–high J_0 values.

Figure 4C shows that the $J(V)$ characteristics are independent of T over the range of T of 8.5–340 K in vacuum (1×10^{-5} bar), which indicates that changing T and the ambient conditions (from 24 °C in air with a relative humidity of 60% to vacuum) of the devices did not change their electrical characteristics. In agreement with Figure 3B, CP behaves like a metal and does not introduce significant temperature-dependent effects, unlike large-area junctions based on protective barriers of conductive polymers[6,68,69] or rGO[12,14,31,33,71] (expect for highly optimized rGO synthesis and thin film fabrication;[72] Table 1).

Extraction of Charge Transport Parameters. To establish whether CP compromises molecular effects, we extracted the transport parameters using a previously reported method[17] based on a second-order Taylor expansion (parabolic model, see section S5)

$$I = G_{eq} \times V\left[1 + s\frac{V}{V_0} + \left(\frac{V}{V_0}\right)^2\right] \quad (5)$$

Here, G_{eq}, V_0, and S are the equilibrium conductance (conductance at zero bias), scaling voltage, and asymmetry factor (S = 0 for symmetric J–V traces), respectively. The parameter V_0 is closely related to the so-called transition voltage, V_t, but the latter depends strongly on the chosen model (e.g., a parabolic model yields $V_t \equiv V_0$, but this identity fails for a single-level Landauer model[17]), while the former is robust and can be seen as a figure of merit.

To investigate how the applied voltage perturbs the conductance from its equilibrium level, as described by the term in square brackets in eq 5, we used the normalized differential conductance, NDC, presentation[15,16]

$$\mathrm{NDC} = \frac{dI}{dV}\cdot\frac{V}{I} = \frac{d\log I}{d\log V} \quad (6)$$

which is a mathematical tool to exclude the orders of magnitude variation in G_{eq} as well as to obtain a quantitative

https://dx.doi.org/10.1021/jacs.9b12424
J. Am. Chem. Soc. 2020, 142, 3513–3524

measure of the $I-V$ power dependence.[15] Figure 4D shows the average NDC curves along with fits to the parabolic approximation (an NDC derivation of eq 5). We performed NDC analysis for all of the individual $J-V$ traces obtained from the junctions with SC_n SAMs with $n = 4-14$ (evens only), and Figure S12 shows the distribution of NDC values of all of the junctions in 2D heat map plots. Figures S13−15 show the histograms of all of the parameters extracted from the NDC analysis for all of the $J-V$ curves. The NDC curves are highly symmetrical with $S = 0.03-0.05$ (Figure S13); this low value of S indicates that the CP layer did not result in significant dipoles across the interfaces as expected from the similarity of the work functions of CP (4.34 ± 0.05 eV; Figure 3A) and Au coated with an alkanethiolate SAM (4.2 eV).[63]

The shape of the NDC curves changes significantly as a function of n: for short molecules ($n = 4$) NDC does not exceed 1.12, indicating a close to linear $I-V$ response; the NDC values increase with the molecular length and reach a maximal NDC = 2.4 for $n = 14$ which is close to NDC = 3, the highest NDC value within the parabolic approximation (Figure S16 shows the corresponding $J(V)$ plots on a linear scale). This is indirect support for the high quality of the junction because both series and shunt resistance attenuate the NDC values toward 1 (simple resistor).

The variation of NDC with molecular length is reflected in the value of V_0, which is reciprocally proportional to the number of carbons, n (see Figure 5A). The variation of V_0 with molecular length indicates that the applied voltage falls mostly on the molecular body, yielding a so-called trapezoidal barrier as schematically illustrated in Figure S17, where the molecular transmission probability τ_m varies with the applied voltage. This is in contrast to the prevailing approach where the voltage only widens the accessible energy window of a voltage-independent transmission probability (for an exception see ref 78). Such energy-window-view suits situations with an effective buffer between the nano-object and at least one of the contacts as is the case for STM experiments (Figure S17C) or both contacts such as encountered for junctions with (molecular) quantum dots (Figure S17A), where the majority of the potential drops at the interfaces. In contrast, molecular junctions, especially those with saturated molecules like alkanes, have a very low transmission probability, which is, in principle, lower than the coupling across the interface, especially for two chemisorbed contacts[52,58] (i.e., $\tau_{mol} \ll \tau_C$). However, in practice, the exact voltage partition depends on various factors and may significantly drop on the interfaces in cases of, for instance, poorly conducting PL, nonmetallic substrates (e.g., silicon[79]), and low-force CP-AFM and possibly also for contacts with a very large surface roughness including cone-shaped GaO_x/EGaIn contacts (see ref 60 for details).

The junctions we report here provide a unique example of the "idealized" case, where the alkyl chains serve as the dominant insulating part, and therefore, their voltage response varies with the molecular length. The majority of modern theoretical treatments do not consider length explicitly, and therefore, we have to revert to the Simmons model,[80] which predicts a reciprocal scaling voltage−length dependency as given in eq 7[15,17,81]

$$V_0 = 9.8\varepsilon/\beta d \tag{7}$$

where ε is the energy barrier for tunneling (ε in eV). Figure 5A shows the linear relation between V_0 and $1/d$ for the junctions with d from 6 to 14 with a slope $\varepsilon = 1.7 \pm 0.17$ eV; junctions

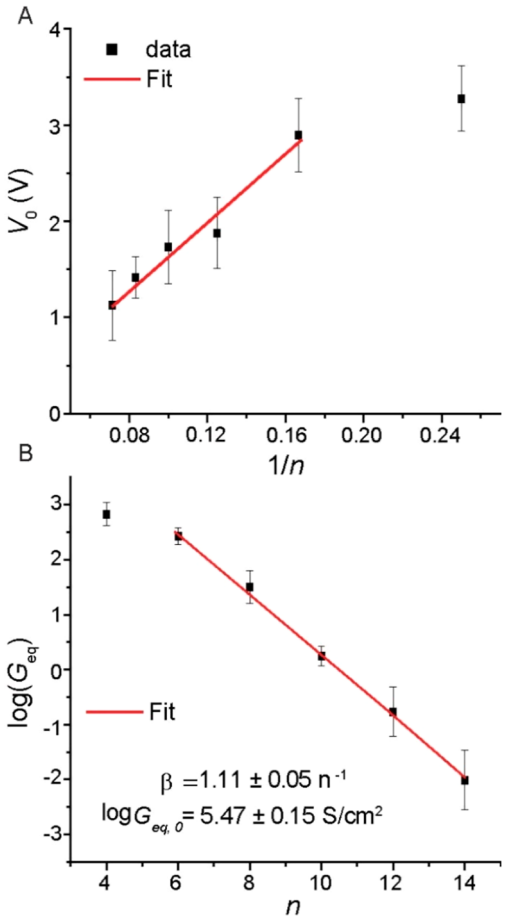

Figure 5. (A) Plot of transition voltage (V_0) vs $1/n$ (error bars represent the standard deviation from five independent $J-V$ traces). (B) Plot of $\log(G_{eq})$ vs n; solid line is a fit to eq 8.

with SC_4 SAMs have a resistance that is very close to the resistance of junctions without SAMs (Figure 4B) and therefore deviates from the linear relation in Figure 5A. While this value may appear low, it agrees with the distance between the energy of the LUMO and the Fermi level for alkyl−S−Au SAMs as measured by inverse photoemission spectroscopy (IPES),[82] which is similar to that measured for alkyl−Si SAMs.[83] The rather low barrier is because the electron-rich substrate stabilizes the molecular energy levels (also known as energy-level renormalization) which acts to reduce the HOMO−LUMO gap from ∼9 eV in vacuum to ∼7 eV (i.e., renormalization factor of 1.3).[82,83] For EGaIn junctions we have reported a renormalization factor of 1.5.[84]

The value of β is remarkably insensitive to the shape of the potential profile (Figure 5); however, nonlinear current−voltage characteristics can only be observed when the voltage drops significantly over the molecules inside the junction. Our observation that the voltage drops mostly on the SAM implies that the R_s of the CP is sufficiently low and that τ_C is sufficiently high,[60] so that molecular effects dominate the electrical properties of the junctions. Alkyl chains by themselves have a rather weak voltage effect on the transmission (parabolic dependence), yet the evidence that the voltage is not "lost" on the contacts makes CP a promising contact for other types of functional molecules.

Effective Contact Area. The low contact resistance of CP (in terms of both R_s and τ_C) explains both the voltage drop on

https://dx.doi.org/10.1021/jacs.9b12424
J. Am. Chem. Soc. 2020, 142, 3513−3524

the molecules (Figures 4D and 5A) and, at least in part, the high J_0 values as defined in eq 3 (Figure 4B and Table 1). The value of J_0, however, also depends on A_f. We estimated the number of molecules N contributing to the net conductance from the G_{eq} values extracted from the parabolic fitting (eq 5). The G_{eq} is linearly proportional to the number of molecules, N in molecules/cm^2 (i.e., parallel conductors), or effective contact area and exponentially inversely proportional to d (in n) as described by eq 8.

$$G_{eq} \equiv G(0\ \mathrm{V}) = NG_0\tau_C e^{-\beta_{eq} n} \tag{8}$$

Figure 5B shows a plot of $\log(G_{eq})$ vs n along with a fit to an exponential decay, eq 8, to obtain $\beta_{eq} = 1.11 \pm 0.05\ n^{-1}$ and $\log G_{eq,0} = 5.47 \pm 0.15$ S/cm^2. The value of β_{eq} is close to the value of β obtained from the $J(V)$ curves using eq 2 (Figure 4B). The values of N were used to determine the values of A_f, which are listed in Table 1. The table shows that CP forms contacts with about 2 orders of magnitude higher effective contact areas than junctions with cone-shaped EGaIn top contacts. This observation is in agreement with the experimentally determined values of A_f of 10^{-2} (Figure S6). These results indicate that the relatively high value of A_f, the high τ_C, and the low R_s all lead to the large value of $\log_{10}|J_0| = 6.20 \pm 0.53$ A/cm^2. Correction of the experimental value for the effective electrical contact area gives $\log_{10}|J_0| = \sim 8.2$ A/cm^2, which is close to the values observed in single-molecule junctions (Table 1), indicating that there is room for improvement by reducing the surface roughness by, for example, reducing the size of the graphite flakes of the CP.

Contact Resistance. To identify the factor that contributes to the contact resistance, we characterized the Au^{TS}–SC$_n$//CP//Au junctions with n = 10, 12, and 14 by impedance spectroscopy using a sinusoidal perturbation of 30 mV as a function of frequency (10^2–10^6 Hz) at 0 V following previously reported procedures (see SI for more details).[85] Figure 6A shows the frequency dependence of the modulus of the complex impedance ($|Z|$) which increases over 3 orders of magnitude with changing n from 10 to 14. The solid lines in Figure 6A are fits to the equivalent circuit shown in the inset, which consists of a resistance (R_s) in series with a parallel combination of a constant-phase element (CPE) and a resistor representing the resistance of the SAM (R_{SAM}). In other words, the CP–PL did not cause significant capacitive effects and only adds to the value of R_s, which confirms its metallic-like behavior. The phase ($-\phi$) increases from 0° to 84 ± 5° (error represents the standard deviation from three different junctions) at high frequencies (Figure 6B) when the impedance is dominated by the capacitive reactance of the junction. In Section S6 we show in detail that the junctions do not suffer from stray capacitances or leakage currents across the AlO_x layer, and the relative dielectric constant of the SAM of 3.1 ± 0.4 is within error the same as previously reported values;[68,85] these observations further demonstrate that the junctions are dominated by molecular effects.

The value of R_{SAM} is given by eq 9

$$R_{SAM} = R_C e^{\beta d} \tag{9}$$

where R_C is inversely proportional to $G_{eq,0}$, $R_C \propto 1/G_{eq,0}$. Figure 6C shows R_{SAM} as a function of d along with a fit to eq 9 to yield $\beta = 0.93 \pm 0.07\ n^{-1}$, which is close to the value obtained from the $J(V)$ curves discussed above. The value of R_s is the sum of the resistance across the CP layer, the metal

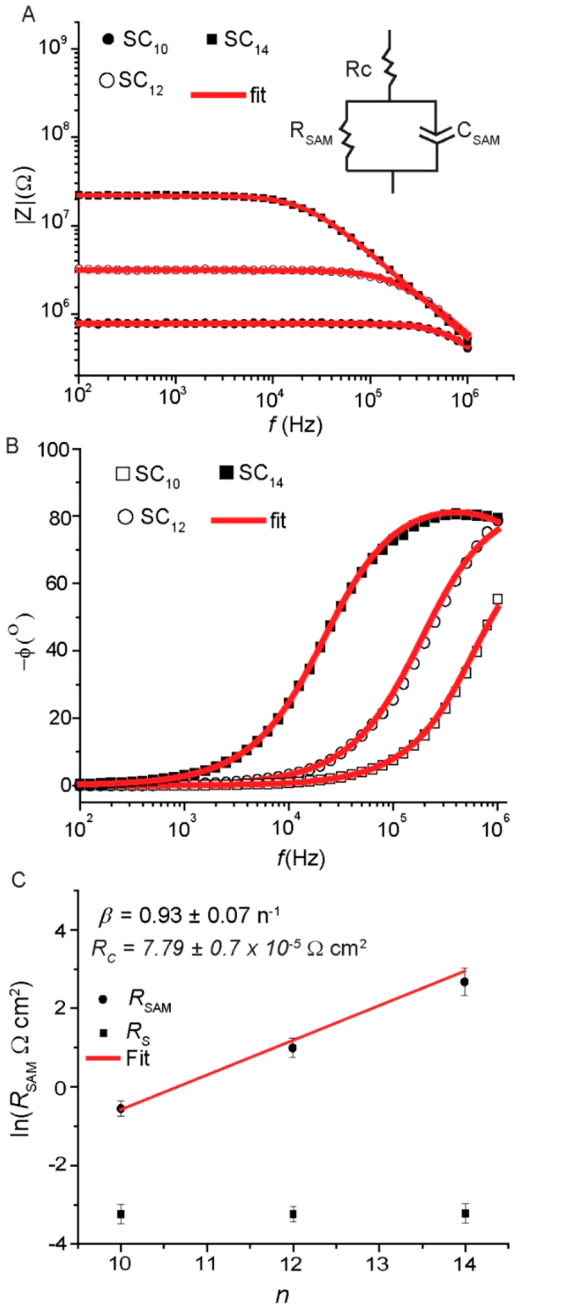

Figure 6. (A) Frequency dependency of $|Z|$ of the junctions at zero bias for micropore device with SAM of SC$_n$ with n = 10, 12, or 14. (B) Corresponding phase angle (ϕ) vs frequency plots. (C) Resistance of the SAM (R_{SAM}) and the contact resistance (R_C) vs the number of carbons; red line is a fit to eq 9.

electrodes, and all of the cables that were used to connect the devices to the electrometers. We hypothesize that R_s is mainly dominated by the internal resistance of the CP layer. To prove our hypothesis, the resistance (1.44×10^{-3} Ω cm^2) of the Au^{TS}//CP//Au junction was determined from the linear low-bias regime over ±0.2 V, Figure 3D. The value of R_s is independent of the thickness of the SAM and has a value of 3.9 ± 0.30 × 10^{-3} Ω cm^2 (Figure 6C). We did not measure all of the individual resistances of the different interfaces, but the value of R_s is roughly equal to that of the resistance of the Au^{TS}//CP//Au junction from which we conclude that R_s is dominated by the internal resistance of the CP layer. The

https://dx.doi.org/10.1021/jacs.9b12424
J. Am. Chem. Soc. 2020, 142, 3513–3524

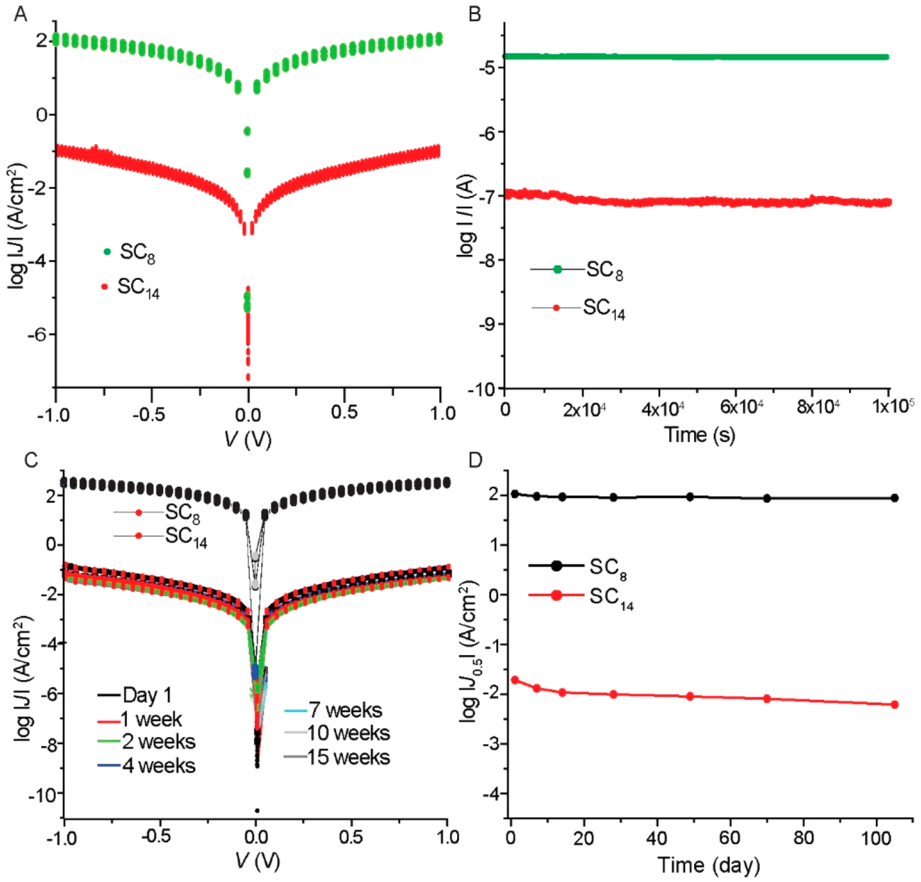

Figure 7. Stabilities of the junctions with SAMs SC_8, SC_{14}, and SC_{14}. (A) 2000 $J(V)$ curves measured by continuously sweeping the bias between +1.0 and −1.0 V. (B) Retention characteristics at +1.0 V for 1.02×10^5 s while measuring the current at 15 s intervals. (C) $J(V)$ curves of junctions and (D) value of J at 0.5 V measured within 1 day after fabrication and after aging for 15 weeks in ambient conditions (at 24 °C in air, relative humidity of 60%).

intercept of the fit with eq 9 gives the contact resistance of the CP with the SAM, R_C (which also includes contributions from the Au−S contact), which is associated with tunneling across the SAM//electrode interfaces and directly relates to τ_C (eq 3). We found $R_C = 7.79 \pm 0.7 \times 10^{-5}$ Ω cm^2. For the sake of consistency, we wish to point out that $R_C \times R_s = 3.04 \pm 0.02 \times 10^{-7}$ Ω cm^2 ($1/(R_s \times R_C) = 3.29 \pm 0.02 \times 10^6$ A/cm^2), which is within error the same as the value of J_0 ($10^{6.2\pm0.53}$) measured with dc methods discussed earlier. Finally, we note that the value of R_s is independent of n, indicating that variations in the Au^{TS}−SC_n//CP//Au between experiments are insignificant.

Stability of the Junctions. We tested the stability of the junctions with SAMs of SC_8 or SC_{14} by continuous cycling of the voltage from 0 to +1.0 to −1.0 to 0.0 V 2000 times (Figure 7A) by measuring the current retention at +1.0 V for 1.02×10^5 s (Figure 7B) and aging in ambient conditions for 15 weeks (at 24 °C in air with a relative humidity of 60%; Figure 7C). The junctions are stable against voltage cycling and retain their currents well, but the currents decreased with time during aging (Figure 7D). Junctions with SAMs of $n = 8$ are the most stable, and the currents did not decrease significantly, but for junctions with $n = 14$, the decrease of J after 15 weeks is a factor of 3.1. We believe that the limiting factor is the gold−thiolate bond which is known to oxidize with time.[86,87] It is well known that the Au−S bond readily oxidizes in air to form sulfonates, sulfates, and sulfite species.[86−88] Oxidation in air, however, does not result in removal of the SAMs as in the case of UV-induced oxidation,[86] although it will affect the quality of the SAM. We believe that the junctions with $n = 8$ do not seem to be sensitive against oxidation of the gold−thiolate bond due to their liquid-like nature which results in self-repair and compensates for the disorder as the molecules in the SAMs have the freedom to rotate into the defective site.[89] In contrast, thick crystalline-like SAMs are rigid, and the molecules lack the freedom to compensate for defects. Consequently, junctions with thick SAMs are more sensitive to defects than junctions with thin SAMs.

CONCLUSIONS

We report a procedure to fabricate high-quality large-area molecular junctions with commercially available carbon paint as a new protective layer which offers the following benefits: (i) It is solution processable, eliminating the need for complicated transfer steps unlike protective layers based on graphene, (ii) it is metallic in behavior resulting in a very low contact resistance (Table 1), (iii) it does not induce unwanted temperature effects in the junction characteristics over a wide range of temperatures (8.5−340 K) unlike protective barriers based on conductive polymers or (reduced) graphene oxides, (iv) it results in highly stable junctions with excellent retention (for 1.2×10^5 s) and bias-stressing characteristics (2000 current−voltage cycles), (v) it does not contain polymers which could intercalate with the SAM obscuring molecular effects and introduce high resistances, and (vi) it results in junctions that are completely dominated by molecular effects

https://dx.doi.org/10.1021/jacs.9b12424
J. Am. Chem. Soc. 2020, 142, 3513−3524

with good reproducibilities and 100% yield in nonshorting junction yields. For all of these reasons, we conclude that the CP is potentially an interesting protective barrier material for applications in molecular electronics.

Normally, only the overall contact resistance (or values of J_0) is reported, but it is unclear which factors dominate the overall contact resistance. A detailed NDC analysis of the junction characteristics in conjunction with impedance spectroscopy allowed us to identify three factors that contribute to the overall contact resistance (or J_0). In our junctions, the overall contact resistance was low because the CP layer forms an intimate contact with the SAMs, resulting in high tunneling probabilities across the SAM//CP interface (high τ_C values, eq 1) and high effective contact areas (A_p, or the number of molecules participating in charge transport N, eq 1). Although the resistance across the CP layer, R_s, still contributes significantly to the overall contact resistance limiting the SAM thickness that can be measured to SC_4, we believe R_s can be lowered by reducing the thickness of the CP layer (here we used 1 μm) by improving the formulation of the CP consisting of small graphite flakes, for instance, allowing one to spin coat thinner CP films. Smaller graphite flakes could also improve the effective contact area the CP makes with the SAMs, especially relative to graphene-based protective layers as graphene buckles,[90] resulting in areas of noncontact. These new insights into the factors that contribute to the overall contact resistance help to improve the design of junction platforms and guide future experiments where it is important to measure molecules with very low tunneling resistances (or high values of τ_C in eq 1).

■ ASSOCIATED CONTENT

Supporting Information

The Supporting Information is available free of charge at https://pubs.acs.org/doi/10.1021/jacs.9b12424.

Experimental details, profilometer height profile of the spin-coated CP layer, AFM, XPS, and SEM for different batches of the CP, resistance of the CP layer, statistical analysis of $J(V)$ measurements and transport parameters extracted with NDC analysis, and error analysis of impedance spectroscopy (PDF)

■ AUTHOR INFORMATION

Corresponding Authors

Ayelet Vilan − *Department of Chemical and Biological Physics, Weizmann Institute of Science, Rehovot 76100, Israel;* orcid.org/0000-0001-5126-9315; Email: ayelet.vilan@weizmann.ac.il

Christian A. Nijhuis − *Department of Chemistry and Centre for Advanced 2D Materials, National University of Singapore, Singapore 117543 Singapore;* orcid.org/0000-0003-3435-4600; Email: chmnca@nus.edu.sg

Authors

Senthil Kumar Karuppannan − *Department of Chemistry, National University of Singapore, Singapore 117543 Singapore*

Esther Hui Lin Neoh − *Department of Chemistry, National University of Singapore, Singapore 117543 Singapore*

Complete contact information is available at: https://pubs.acs.org/10.1021/jacs.9b12424

Notes

The authors declare no competing financial interest.

■ ACKNOWLEDGMENTS

The Prime Minister's Office, Singapore under its Medium Sized Centre Program is acknowledged for supporting this research. We also acknowledge the Ministry of Education (MOE) for supporting this research under award No. MOE2015-T2-2-134.

■ REFERENCES

(1) Vilan, A.; Aswal, D.; Cahen, D. Large-Area, Ensemble Molecular Electronics: Motivation and Challenges. *Chem. Rev.* **2017**, *117*, 4248−4286.

(2) Metzger, R. M. Unimolecular Electronics. *Chem. Rev.* **2015**, *115*, 5056−5115.

(3) Van Hal, P. A.; Smits, E. C. P.; Geuns, T. C. T.; Akkerman, H. B.; De Brito, B. C.; Perissinotto, S.; Lanzani, G.; Kronemeijer, A. J.; Geskin, V.; Cornil, J.; Blom, P. W. M.; De Boer, B.; De Leeuw, D. M. Upscaling, Integration and Electrical Characterization of Molecular Junctions. *Nat. Nanotechnol.* **2008**, *3*, 749−754.

(4) Xiang, D.; Wang, X.; Jia, C.; Lee, T.; Guo, X. Molecular-Scale Electronics: From Concept to Function. *Chem. Rev.* **2016**, *116*, 4318−4440.

(5) Jeong, H.; Kim, D.; Xiang, D.; Lee, T. High-Yield Functional Molecular Electronic Devices. *ACS Nano* **2017**, *11*, 6511−6548.

(6) Neuhausen, A. B.; Hosseini, A.; Sulpizio, J. A.; Chidsey, C. E. D.; Goldhaber-Gordon, D. Molecular Junctions of Self-Assembled Monolayers with Conducting Polymer Contacts. *ACS Nano* **2012**, *6*, 9920−9931.

(7) Milani, F.; Grave, C.; Ferri, V.; Samorì, P.; Rampi, M. A. Ultrathin π-Conjugated Polymer Films for Simple Fabrication of Large-Area Molecular Junctions. *ChemPhysChem* **2007**, *8*, 515−518.

(8) Morteza Najarian, A.; Szeto, B.; Tefashe, U. M.; McCreery, R. L. Robust All-Carbon Molecular Junctions on Flexible or Semi-Transparent Substrates Using "Process-Friendly" Fabrication. *ACS Nano* **2016**, *10*, 8918−8928.

(9) Chung, D. D. L. Electrical Applications of Carbon Materials. *J. Mater. Sci.* **2004**, *39*, 2645−2661.

(10) Puebla-Hellmann, G.; Venkatesan, K.; Mayor, M.; Lörtscher, E. Metallic Nanoparticle Contacts for High-Yield, Ambient-Stable Molecular-Monolayer Devices. *Nature* **2018**, *559*, 232−235.

(11) Wang, G.; Kim, Y.; Choe, M.; Kim, T.-W.; Lee, T. A New Approach for Molecular Electronic Junctions with a Multilayer Graphene Electrode. *Adv. Mater.* **2011**, *23*, 755−760.

(12) Li, T.; Hauptmann, J. R.; Wei, Z.; Petersen, S.; Bovet, N.; Vosch, T.; Nygård, J.; Hu, W.; Liu, Y.; Bjørnholm, T.; Nørgaard, K.; Laursen, B. W. Solution-Processed Ultrathin Chemically Derived Graphene Films as Soft Top Contacts for Solid-State Molecular Electronic Junctions. *Adv. Mater.* **2012**, *24*, 1333−1339.

(13) Buzaglo, M.; Shtein, M.; Kober, S.; Lovrinčić, R.; Vilan, A.; Regev, O. Critical Parameters in Exfoliating Graphite into Graphene. *Phys. Chem. Chem. Phys.* **2013**, *15*, 4428−4435.

(14) Seo, S.; Min, M.; Lee, J.; Lee, T.; Choi, S. Y.; Lee, H. Solution-Processed Reduced Graphene Oxide Films as Electronic Contacts for Molecular Monolayer Junctions. *Angew. Chem., Int. Ed.* **2012**, *51*, 108−112.

(15) Vilan, A.; Cahen, D.; Kraisler, E. Rethinking Transition Voltage Spectroscopy within a Generic Taylor Expansion View. *ACS Nano* **2013**, *7*, 695−706.

(16) Vilan, A. Revealing Tunnelling Details by Normalized Differential Conductance Analysis of Transport across Molecular Junctions. *Phys. Chem. Chem. Phys.* **2017**, *19*, 27166−27172.

(17) Vilan, A. Analyzing Molecular Current-Voltage Characteristics with the Simmons Tunneling Model: Scaling and Linearization. *J. Phys. Chem. C* **2007**, *111*, 4431−4444.

(18) Lovrinčić, R.; Kraynis, O.; Har-Lavan, R.; Haj-Yahya, A. E.; Li, W.; Vilan, A.; Cahen, D. A New Route to Nondestructive Top-

Contacts for Molecular Electronics on Si: Pb Evaporated on Organic Monolayers. *J. Phys. Chem. Lett.* **2013**, *4*, 426−430.
(19) Haick, H.; Niitsoo, O.; Ghabboun, J.; Cahen, D. Electrical Contacts to Organic Molecular Films by Metal Evaporation: Effect of Contacting Details. *J. Phys. Chem. C* **2007**, *111*, 2318−2329.
(20) Bonifas, A. P.; McCreery, R. L. Soft Au, Pt and Cu Contacts for Molecular Junctions through Surface-Diffusion-Mediated Deposition. *Nat. Nanotechnol.* **2010**, *5*, 612−617.
(21) Metzger, R. M.; Xu, T.; Peterson, I. R. Electrical Rectification by a Monolayer of Hexadecylquinolinium Tricyanoquinodimethanide Measured between Macroscopic Gold Electrodes. *J. Phys. Chem. B* **2001**, *105*, 7280−7290.
(22) Yaffe, O.; Scheres, L.; Segev, L.; Biller, A.; Ron, I.; Salomon, E.; Giesbers, M.; Kahn, A.; Kronik, L.; Zuilhof, H.; Vilan, A.; Cahen, D. Hg/Molecular Monolayer−Si Junctions: Electrical Interplay between Monolayer Properties and Semiconductor Doping Density. *J. Phys. Chem. C* **2010**, *114*, 10270−10279.
(23) Slowinski, K.; Chamberlain, R. V.; Miller, C. J.; Majda, M. Through-Bond and Chain-to-Chain Coupling. Two Pathways in Electron Tunneling through Liquid Alkanethiol Monolayers on Mercury Electrodes. *J. Am. Chem. Soc.* **1997**, *119*, 11910−11919.
(24) Dickey, M. D.; Chiechi, R. C.; Larsen, R. J.; Weiss, E. A.; Weitz, D. A.; Whitesides, G. M. Eutectic Gallium-Indium (EGaIn): A Liquid Metal Alloy for the Formation of Stable Structures in Microchannels at Room Temperature. *Adv. Funct. Mater.* **2008**, *18*, 1097−1104.
(25) Nijhuis, C. A.; Reus, W. F.; Barber, J. R.; Whitesides, G. M. Comparison of SAM-Based Junctions with Ga 2 O 3 /EGaIn Top Electrodes to Other Large-Area Tunneling Junctions. *J. Phys. Chem. C* **2012**, *116*, 14139−14150.
(26) Akkerman, H. B.; Blom, P. W. M.; de Leeuw, D. M.; de Boer, B. Towards Molecular Electronics with Large-Area Molecular Junctions. *Nature* **2006**, *441*, 69−72.
(27) Jang, Y.; Jeong, H.; Kim, D.; Hwang, W.-T.; Kim, J.-W.; Jeong, I.; Song, H.; Yoon, J.; Yi, G.-C.; Jeong, H.; Lee, T. Electrical Characterization of Benzenedithiolate Molecular Electronic Devices with Graphene Electrodes on Rigid and Flexible Substrates. *Nanotechnology* **2016**, *27*, 145301.
(28) Ambrosi, A.; Pumera, M. The CVD Graphene Transfer Procedure Introduces Metallic Impurities Which Alter the Graphene Electrochemical Properties. *Nanoscale* **2014**, *6*, 472−476.
(29) Suk, J. W.; Kitt, A.; Magnuson, C. W.; Hao, Y.; Ahmed, S.; An, J.; Swan, A. K.; Goldberg, B. B.; Ruoff, R. S. Transfer of CVD-Grown Monolayer Graphene onto Arbitrary Substrates. *ACS Nano* **2011**, *5*, 6916−6924.
(30) Seo, S.; Min, M.; Lee, J.; Lee, T.; Choi, S. Y.; Lee, H. Solution-Processed Reduced Graphene Oxide Films as Electronic Contacts for Molecular Monolayer Junctions. *Angew. Chem., Int. Ed.* **2012**, *51*, 108−112.
(31) Li, T.; Jevric, M.; Hauptmann, J. R.; Hviid, R.; Wei, Z.; Wang, R.; Reeler, N. E. A.; Thyrhaug, E.; Petersen, S.; Meyer, J. A. S.; Bovet, N.; Vosch, T.; Nygård, J.; Qiu, X.; Hu, W.; Liu, Y.; Solomon, G. C.; Kjaergaard, H. G.; Bjørnholm, T.; Nielsen, M. B.; Laursen, B. W.; Nørgaard, K. Ultrathin Reduced Graphene Oxide Films as Transparent Top-Contacts for Light Switchable Solid-State Molecular Junctions. *Adv. Mater.* **2013**, *25*, 4164−4170.
(32) Eda, G.; Fanchini, G.; Chhowalla, M. Large-Area Ultrathin Films of Reduced Graphene Oxide as a Transparent and Flexible Electronic Material. *Nat. Nanotechnol.* **2008**, *3*, 270−274.
(33) Kühnel, M.; Petersen, S. V.; Hviid, R.; Overgaard, M. H.; Laursen, B. W.; Nørgaard, K. Monolayered Graphene Oxide as a Low Contact Resistance Protection Layer in Alkanethiol Solid-State Devices. *J. Phys. Chem. C* **2018**, *122*, 9731−9737.
(34) Wang, C.; Xia, K.; Wang, H.; Liang, X.; Yin, Z.; Zhang, Y. Advanced Carbon for Flexible and Wearable Electronics. *Adv. Mater.* **2019**, *31*, 1801072.
(35) Hatala, M.; Gemeiner, P.; Hvojnik, M.; Mikula, M. The Effect of the Ink Composition on the Performance of Carbon-Based Conductive Screen Printing Inks. *J. Mater. Sci.: Mater. Electron.* **2019**, *30*, 1034−1044.
(36) TED Pella, I. P.O. Box 492477, Redding, CA 96049-2477; https://www.tedpella.com/.
(37) SPI Supplies Division Structure Probe, Inc., 206 Garfield Ave., West Chester, PA 19380; https://www.2spi.com/.
(38) Phillips, C.; Al-Ahmadi, A.; Potts, S. J.; Claypole, T.; Deganello, D. The Effect of Graphite and Carbon Black Ratios on Conductive Ink Performance. *J. Mater. Sci.* **2017**, *52*, 9520−9530.
(39) Homola, T.; Pospíšil, J.; Krumpolec, R.; Souček, P.; Dzik, P.; Weiter, M.; Černák, M. Atmospheric Dry Hydrogen Plasma Reduction of Inkjet-Printed Flexible Graphene Oxide Electrodes. *ChemSusChem* **2018**, *11*, 941−947.
(40) Schmiedova, V.; Pospisil, J.; Kovalenko, A.; Ashcheulov, P.; Fekete, L.; Cubon, T.; Kotrusz, P.; Zmeskal, O.; Weiter, M. Physical Properties Investigation of Reduced Graphene Oxide Thin Films Prepared by Material Inkjet Printing. *J. Nanomater.* **2017**, *2017*, 1−8.
(41) Ma, Y.; Zhi, L. Graphene-Based Transparent Conductive Films: Material Systems, Preparation and Applications. *Small Methods* **2019**, *3*, 1800199.
(42) Worsley, R.; Pimpolari, L.; McManus, D.; Ge, N.; Ionescu, R.; Wittkopf, J. A.; Alieva, A.; Basso, G.; MacUcci, M.; Iannaccone, G.; Novoselov, K. S.; Holder, H.; Fiori, G.; Casiraghi, C. All-2D Material Inkjet-Printed Capacitors: Toward Fully Printed Integrated Circuits. *ACS Nano* **2019**, *13*, 54−60.
(43) Parvez, K.; Worsley, R.; Alieva, A.; Felten, A.; Casiraghi, C. Water-Based and Inkjet Printable Inks Made by Electrochemically Exfoliated Graphene. *Carbon* **2019**, *149*, 213−221.
(44) Rattanaweeranon, S.; Limsuwan, P.; Thongpool, V.; Piriyawong, V.; Asanithi, P. Influence of Bulk Graphite Density on Electrical Conductivity. *Procedia Eng.* **2012**, *32*, 1100−1106.
(45) Santhiago, M.; Corrêa, C. C.; Bernardes, J. S.; Pereira, M. P.; Oliveira, L. J. M.; Strauss, M.; Bufon, C. C. B.; Nie, Z.; Nijhuis, C. A.; Gong, J.; Chen, X.; Kumachev, A.; Martinez, A. W.; Narovlyansky, M.; Whitesides, G. M.; Santhiago, M.; Corrêa, C. C.; Bernardes, J. S.; Pereira, M. P.; Oliveira, L. J. M.; Strauss, M.; Bufon, C. C. B. Flexible and Foldable Fully-Printed Carbon Black Conductive Nanostructures on Paper for High-Performance Electronic, Electrochemical, and Wearable Devices. *ACS Appl. Mater. Interfaces* **2017**, *9*, 24365−24372.
(46) Nie, Z.; Nijhuis, C. A.; Gong, J.; Chen, X.; Kumachev, A.; Martinez, A. W.; Narovlyansky, M.; Whitesides, G. M. Electrochemical Sensing in Paper-Based Microfluidic Devices. *Lab Chip* **2010**, *10*, 477−483.
(47) Wang, G.; Kim, T. W.; Jang, Y. H.; Lee, T. Effects of Metal-Molecule Contact and Molecular Structure on Molecular Electronic Conduction in Nonresonant Tunneling Regime: Alkyl versus Conjugated Molecules. *J. Phys. Chem. C* **2008**, *112*, 13010−13016.
(48) Yuan, L.; Jiang, L.; Zhang, B.; Nijhuis, C. A. Dependency of the Tunneling Decay Coefficient in Molecular Tunneling Junctions on the Topography of the Bottom Electrodes. *Angew. Chem., Int. Ed.* **2014**, *53*, 3377−3381.
(49) Jiang, L.; Sangeeth, C. S. S.; Wan, A.; Vilan, A.; Nijhuis, C. A. Defect Scaling with Contact Area in EGaIn-Based Junctions: Impact on Quality, Joule Heating, and Apparent Injection Current. *J. Phys. Chem. C* **2015**, *119*, 960−969.
(50) Xu, B. Measurement of Single-Molecule Resistance by Repeated Formation of Molecular Junctions. *Science (Washington, DC, U. S.)* **2003**, *301*, 1221−1223.
(51) Chen, F.; Li, X.; Hihath, J.; Huang, Z.; Tao, N. Effect of Anchoring Groups on Single-Molecule Conductance: Comparative Study of Thiol-, Amine-, and Carboxylic-Acid-Terminated Molecules. *J. Am. Chem. Soc.* **2006**, *128*, 15874−15881.
(52) Engelkes, V. B.; Beebe, J. M.; Frisbie, C. D. Length-Dependent Transport in Molecular Junctions Based on SAMs of Alkanethiols and Alkanedithiols: Effect of Metal Work Function and Applied Bias on Tunneling Efficiency and Contact Resistance. *J. Am. Chem. Soc.* **2004**, *126*, 14287−14296.
(53) Zhang, Q.; Tao, S.; Fan, Y.; Zhao, C.; Zhao, C.; Su, W.; Dappe, Y. J.; Nichols, R. J.; Yang, L. Technical Effects of Molecule-Electrode Contacts in Graphene-Based Molecular Junctions. *J. Phys. Chem. C* **2018**, *122*, 23200−23207.

https://dx.doi.org/10.1021/jacs.9b12424
J. Am. Chem. Soc. 2020, 142, 3513−3524

(54) Rothemund, P.; Morris Bowers, C.; Suo, Z.; Whitesides, G. M. Influence of the Contact Area on the Current Density across Molecular Tunneling Junctions Measured with EGaIn Top-Electrodes. *Chem. Mater.* **2018**, *30*, 129−137.
(55) Simeone, F. C.; Yoon, H. J.; Thuo, M. M.; Barber, J. R.; Smith, B.; Whitesides, G. M. Defining the Value of Injection Current and Effective Electrical Contact Area for EGaIn-Based Molecular Tunneling Junctions. *J. Am. Chem. Soc.* **2013**, *135*, 18131−18144.
(56) Chen, X.; Hu, H.; Trasobares, J.; Nijhuis, C. A. Rectification Ratio and Tunneling Decay Coefficient Depend on the Contact Geometry Revealed by in Situ Imaging of the Formation of EGaIn Junctions. *ACS Appl. Mater. Interfaces* **2019**, *11*, 21018−21029.
(57) Rothemund, P.; Morris Bowers, C.; Suo, Z.; Whitesides, G. M. Influence of the Contact Area on the Current Density across Molecular Tunneling Junctions Measured with EGaIn Top-Electrodes. *Chem. Mater.* **2018**, *30*, 129−137.
(58) Beebe, J. M.; Engelkes, V. B.; Miller, L. L.; Frisbie, C. D. Contact Resistance in Metal−Molecule−Metal Junctions Based on Aliphatic SAMs: Effects of Surface Linker and Metal Work Function. *J. Am. Chem. Soc.* **2002**, *124*, 11268−11269.
(59) Yan, H.; Bergren, A. J.; McCreery, R. L. All-Carbon Molecular Tunnel Junctions. *J. Am. Chem. Soc.* **2011**, *133*, 19168−19177.
(60) Karuppannan, S. K.; Hongting, H.; Troadec, C.; Vilan, A.; Nijhuis, C. A. Ultrasmooth and Photoresist-Free Micropore-Based EGaIn Molecular Junctions: Fabrication and How Roughness Determines Voltage Response. *Adv. Funct. Mater.* **2019**, *29*, 1904452.
(61) Ulman, A. Formation and Structure of Self-Assembled Monolayers. *Chem. Rev.* **1996**, *96*, 1533−1554.
(62) Cristina, L. J.; Ruano, G.; Salvarezza, R.; Ferrón, J. Thermal Stability of Self-Assembled Monolayers of n -Hexanethiol on Au(111)-(1 × 1) and Au(001)-(1 × 1). *J. Phys. Chem. C* **2017**, *121*, 27894−27904.
(63) Engelkes, V. B.; Beebe, J. M.; Frisbie, C. D. Length-Dependent Transport in Molecular Junctions Based on SAMs of Alkanethiols and Alkanedithiols: Effect of Metal Work Function and Applied Bias on Tunneling Efficiency and Contact Resistance. *J. Am. Chem. Soc.* **2004**, *126*, 14287−14296.
(64) Susi, T.; Pichler, T.; Ayala, P. X-Ray Photoelectron Spectroscopy of Graphitic Carbon Nanomaterials Doped with Heteroatoms. *Beilstein J. Nanotechnol.* **2015**, *6*, 177−192.
(65) Park, S.; An, J.; Jung, I.; Piner, R. D.; An, J.; Li, X.; Velamakanni, A.; Ruoff, R. S.; Park, S.; An, J.; Jung, I.; Piner, R. D.; An, S. J.; Li, X.; Velamakanni, A.; Ruoff, R. S. Colloidal Suspensions of Highly Reduced Graphene Oxide in a Wide Variety of Organic Solvents. *Nano Lett.* **2009**, *9*, 1593−1597.
(66) Marin, B. C.; Root, S. E.; Urbina, A. D.; Aklile, E.; Miller, R.; Zaretski, A. V.; Lipomi, D. J. Graphene−Metal Composite Sensors with Near-Zero Temperature Coefficient of Resistance. *ACS Omega* **2017**, *2*, 626−630.
(67) Reus, W. F.; Nijhuis, C. A.; Barber, J. R.; Thuo, M. M.; Tricard, S.; Whitesides, G. M. Statistical Tools for Analyzing Measurements of Charge Transport. *J. Phys. Chem. C* **2012**, *116*, 6714−6733.
(68) Akkerman, H. B.; Naber, R. C. G.; Jongbloed, B.; van Hal, P. A.; Blom, P. W. M.; de Leeuw, D. M.; de Boer, B. Electron Tunneling through Alkanedithiol Self-Assembled Monolayers in Large-Area Molecular Junctions. *Proc. Natl. Acad. Sci. U. S. A.* **2007**, *104*, 11161−11166.
(69) Park, S.; Wang, G.; Cho, B.; Kim, Y.; Song, S.; Ji, Y.; Yoon, M. H.; Lee, T. Flexible Molecular-Scale Electronic Devices. *Nat. Nanotechnol.* **2012**, *7*, 438−442.
(70) Wimbush, K. S.; Fratila, R. M.; Wang, D.; Qi, D.; Liang, C.; Yuan, L.; Yakovlev, N.; Loh, K. P.; Reinhoudt, D. N.; Velders, A. H.; et al. Bias Induced Transition from an Ohmic to a Non-Ohmic Interface in Supramolecular Tunneling Junctions with Ga 2 O 3 /EGaIn Top Electrodes. *Nanoscale* **2014**, *6*, 11246−11258.
(71) Jeong, H.; Kim, D.; Kim, P.; Rae Cho, M.; Hwang, W.-T.; Jang, Y.; Cho, K.; Min, M.; Xiang, D.; Daniel Park, Y.; Jeong, H.; Lee, T. A New Approach for High-Yield Metal–Molecule–Metal Junctions by Direct Metal Transfer Method. *Nanotechnology* **2015**, *26*, 025601.
(72) Kühnel, M.; Overgaard, M. H.; Hels, M. C.; Cui, A.; Vosch, T.; Nygård, J.; Li, T.; Laursen, B. W.; Nørgaard, K. High-Quality Reduced Graphene Oxide Electrodes for Sub-Kelvin Studies of Molecular Monolayer Junctions. *J. Phys. Chem. C* **2018**, *122*, 25102−25109.
(73) Nurbawono, A.; Liu, S.; Nijhuis, C. A.; Zhang, C. Odd−Even Effects in Charge Transport through Self-Assembled Monolayer of Alkanethiolates. *J. Phys. Chem. C* **2015**, *119*, 5657−5662.
(74) Wang, W.; Lee, T.; Reed, M. Mechanism of Electron Conduction in Self Assembled Alkanethil Monolayer Devices. *Phys. Rev. B: Condens. Matter Mater. Phys.* **2003**, *68*, 035416.
(75) Sayed, S. Y.; Bayat, A.; Kondratenko, M.; Leroux, Y.; Hapiot, P.; McCreery, R. L. Bilayer Molecular Electronics: All-Carbon Electronic Junctions Containing Molecular Bilayers Made with "Click" Chemistry. *J. Am. Chem. Soc.* **2013**, *135*, 12972−12975.
(76) Suzuki, M.; Fujii, S.; Fujihira, M. Measurements of Currents through Single Molecules of Alkanedithiols by Repeated Formation of Break Junction in Scanning Tunneling Microscopy under Ultrahigh Vacuum. *Japanese J. Appl. Physics, Part 1 Regul. Pap. Short Notes Rev. Pap.* **2006**, *45*, 2041−2044.
(77) Haiss, W.; Nichols, R. J.; van Zalinge, H.; Higgins, S. J.; Bethell, D.; Schiffrin, D. J. Formation of Molecular Wires. *Phys. Chem. Chem. Phys.* **2004**, *6*, 4330.
(78) Van Dyck, C.; Ratner, M. A. Molecular Rectifiers: A New Design Based on Asymmetric Anchoring Moieties. *Nano Lett.* **2015**, *15*, 1577−1584.
(79) Vilan, A. Insulator Charging Limits Direct Current across Tunneling Metal-Insulator-Semiconductor Junctions. *J. Appl. Phys.* **2016**, *119*, 014504.
(80) Simmons, J. G. Generalized Formula for the Electric Tunnel Effect between Similar Electrodes Separated by a Thin Insulating Film. *J. Appl. Phys.* **1963**, *34*, 1793−1803.
(81) Huisman, E. H.; Guédon, C. M.; van Wees, B. J.; van der Molen, S. J. Interpretation of Transition Voltage Spectroscopy. *Nano Lett.* **2009**, *9*, 3909−3913.
(82) Qi, Y.; Yaffe, O.; Tirosh, E.; Vilan, A.; Cahen, D.; Kahn, A. Filled and Empty States of Alkanethiol Monolayer on Au (111): Fermi Level Asymmetry and Implications for Electron Transport. *Chem. Phys. Lett.* **2011**, *511*, 344−347.
(83) Yaffe, O.; Qi, Y.; Scheres, L.; Puniredd, S. R.; Segev, L.; Ely, T.; Haick, H.; Zuilhof, H.; Vilan, A.; Kronik, L.; Kahn, A.; Cahen, D. Charge Transport across Metal/Molecular (Alkyl) Monolayer-Si Junctions Is Dominated by the LUMO Level. *Phys. Rev. B: Condens. Matter Mater. Phys.* **2012**, *85*, 045433.
(84) Yuan, L.; Breuer, R.; Jiang, L.; Schmittel, M.; Nijhuis, C. A. A Molecular Diode with a Statistically Robust Rectification Ratio of Three Orders of Magnitude. *Nano Lett.* **2015**, *15*, 5506−5512.
(85) Sangeeth, C. S. S.; Wan, A.; Nijhuis, C. A. Equivalent Circuits of a Self-Assembled Monolayer-Based Tunnel Junction Determined by Impedance Spectroscopy. *J. Am. Chem. Soc.* **2014**, *136*, 11134−11144.
(86) Schoenfisch, M. H.; Pemberton, J. E. Air Stability of Alkanethiol Self-Assembled Monolayers on Silver and Gold Surfaces. *J. Am. Chem. Soc.* **1998**, *120*, 4502−4513.
(87) Vericat, C.; Vela, M. E.; Benitez, G.; Carro, P.; Salvarezza, R. C. Self-Assembled Monolayers of Thiols and Dithiols on Gold: New Challenges for a Well-Known System. *Chem. Soc. Rev.* **2010**, *39*, 1805−1834.
(88) Li, Y.; Huang, J.; McIver, R. T.; Hemminger, J. C. Characterization of Thiol Self-Assembled Films by Laser Desorption Fourier Transform Mass Spectrometry. *J. Am. Chem. Soc.* **1992**, *114*, 2428−2432.
(89) Jiang, L.; Sangeeth, C. S. S.; Yuan, L.; Thompson, D.; Nijhuis, C. A. One-Nanometer Thin Monolayers Remove the Deleterious Effect of Substrate Defects in Molecular Tunnel Junctions. *Nano Lett.* **2015**, *15*, 6643−6649.
(90) Nirmalraj, P. N.; Thodkar, K.; Guerin, S.; Calame, M.; Thompson, D. Graphene Wrinkle Effects on Molecular Resonance States. *npj 2D Mater. Appl.* **2018**, *2*, 8.

https://dx.doi.org/10.1021/jacs.9b12424
J. Am. Chem. Soc. 2020, 142, 3513−3524